Formation of incoherent Σ3{110} twin boundaries through geometrically necessary boundaries in an Al-8Zn alloy subjected to one pass of equal channel angular pressing

Hailong Jia [a], Shenbao Jin [b], Yanjun Li [a,*]

[a] Department of Materials Science and Engineering, Norwegian University of Science and Technology (NTNU), 7491, Trondheim, Norway

[b] School of Materials Science and Engineering, Nanjing University of Science and Technology, Nanjing, 210094, China

*Corresponding author: yanjun.li@ntnu.no (Yanjun Li).

Abstract

For coarse grained (CG) alloys with high stacking fault energies (SFEs), like aluminum, deformation twins can rarely form. Here, we report that Σ3{110} incoherent twin boundaries (ITBs) could be generated in a CG Al-8Zn alloy by one pass of ECAP. A systematic investigation shows that the Σ3{110} ITBs are formed by gradual evolution from geometrically necessary boundaries (GNBs) delineating deformation bands (DBs) by lattice rotation via <111>-twist CSL boundaries. This is a new deformation mechanism in Al alloys, which has never been reported.

Keywords: Aluminum alloys; Equal channel angular pressing (ECAP); Σ3 boundaries; geometrically necessary boundaries (GNBs); Deformation bands

1. Introduction

When a metal is plastically deformed, two types of dislocation structures have been found, i.e., geometrically necessary boundaries (GNBs) and incidental dislocation boundaries (IDBs) [1]. In one grain, GNBs separate regions deformed by different sets of slip systems or by the same sets of slip systems but with different shear strain amplitudes or different strains, forming band structures [2-4]. IDBs are formed by the statistical trapping of glide dislocations and align in a random pattern. In addition to dislocation slip, deformation twinning is also an important deformation mode [5], which has been reviewed by Meyers et al. [6] and by Christian et al. [7]. Compared to nano-crystalline and fine grained materials, nano-twinned metals exhibit extraordinary properties [8], including high yield strength [9-13], enhanced ductility [10, 13], high electrical conductivity [9, 12] and high strain rate sensitivity [10, 11, 14].

The twinning tendency of a face centered cubic (FCC) metal is largely determined by its stacking fault energy (SFE). For example, with high SFE, coarse grained FCC metals such as Al and Ni are normally deformed by dislocation slip, while FCC metals with low SFE such as Ag are primarily deformed by twinning. However, for coarse grained FCC metals, deformation twinning has been observed under some extreme deformation conditions, such as at crack tips [15, 16] and during high strain rate deformation at cryogenic temperatures [12, 17]. Meanwhile, deformation twinning has been shown to be possible in nano-crystalline materials [18-22], which is due to partial dislocation emissions from grain boundaries (GBs) [21, 22].

It has been proposed that the SFE of Al-Mg alloys decreases with increasing Mg contents [23]. However, a recent first principles calculation based on density function theory (DFT) shows that an addition of Mg in Al can only slightly decrease the SFE and thus the twinning ability is slightly improved [24]. This has been confirmed by an experimental study on an Al-7Mg alloy subjected to dynamic plastic deformation (DPD) under a strain rate of $\sim 10^2$ s^{-1} [25], in which no deformation twins could be found. Instead, a significant fraction of $\Sigma 3$ incoherent twin boundaries (ITBs) have formed, which was proposed to be gradually evolved from low angle deformation bands (DBs) through <111>-twist CSL boundaries [25]. This has been attributed to the special planar glide deformation mode of the Al-7Mg alloy and the high strain rate introduced by DPD.

Equal channel angular pressing (ECAP) has been one of the most important severe plastic deformation (SPD) methods to produce ultrafine grained (UFG) Al and Al alloys. A main focus has been put on the grain refinement mechanism and mechanical properties of the UFG materials [26-29], while the fundamental study on the deformation behavior has been mostly based on single crystals of low alloyed Al alloys [30, 31]. In this paper, we report that a significant fraction of $\Sigma 3\{110\}$ ITBs could form by a special deformation mechanism in an Al-8Zn alloy deformed by conventional ECAP (strain rate, $\sim 2 \times 10^{-2}$ s^{-1}), which has never been reported in ECAP processed Al alloys.

2. Experimental

The material used in the present work was an Al-8 wt.% Zn alloy produced by melting commercial purity Al and Zn. Note that 0.5 wt.% Al-5Ti-1B grain refiner was added into the melt in

order to get fine grains. As illustrated in Fig. 1(a), the as-cast Al-8Zn alloy comprises a granular α-Al grain structure. Fig. 1(b) shows the grain size distribution chart and the average grain size is measured to be ~50 μm.
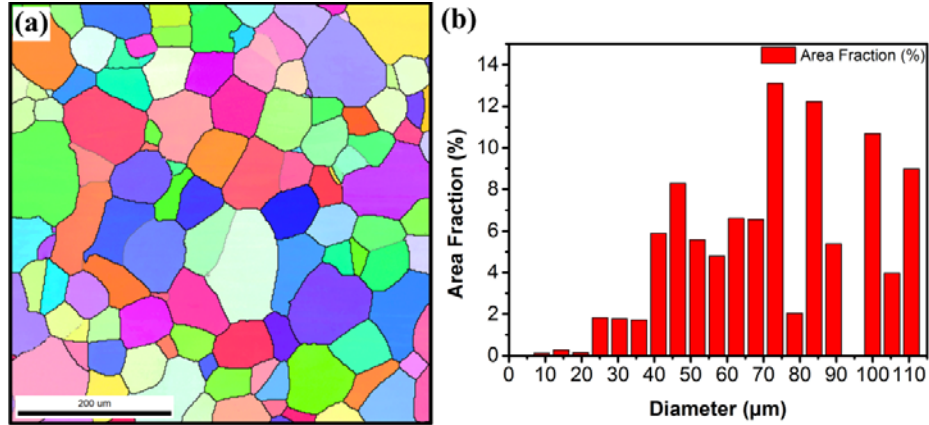

Fig. 1. Microstructures of the as-cast Al-8Zn alloy. (a) EBSD map and (b) grain size distribution chart.

The as-cast ingots were machined into bars with dimensions of 100 mm × 19.5 mm × 19.5 mm. Before ECAP, the bars were coated with a thin layer of a graphite lubricant to lower the friction during ECAP. Then, these bars were processed by ECAP though a 90˚ die (Fig. 2(a)) at room temperature (RT), which leads to an imposed equivalent strain of ~1.0 per pass [27, 32].
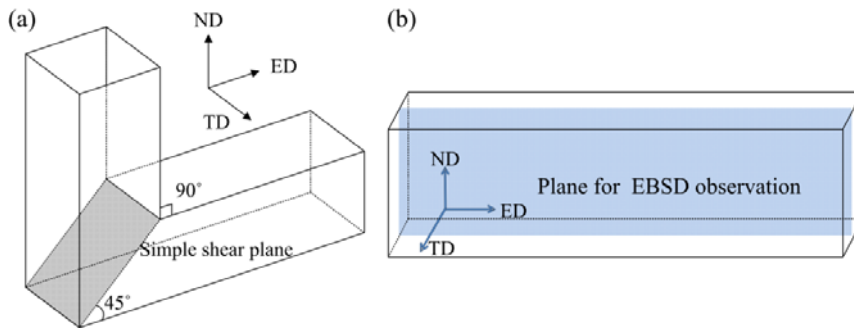

Fig. 2. (a) Schematic diagram of the ECAP die, (b) sketch of the sample for ECAP and the region for EBSD observation is also indicated. ND, TD and ED are abbreviations of the normal, transverse and extrusion directions, respectively.

As shown in Fig. 2(b), samples for microstructure observation were cut from the uniformly deformed region of the ECAP processed bars in the longitudinal section. The as-deformed structure was characterized by electron backscatter diffraction (EBSD). Samples for EBSD were electro-

polished using a solution of 80% C_2H_5OH + 20% $HClO_4$ at 20 V for 15-17 s at -30 ˚C. EBSD was performed by using a Hitachi SU-6600 field emission gun SEM (FEG-SEM) equipped with a Nordif EBSD detector and TSL OIM software.

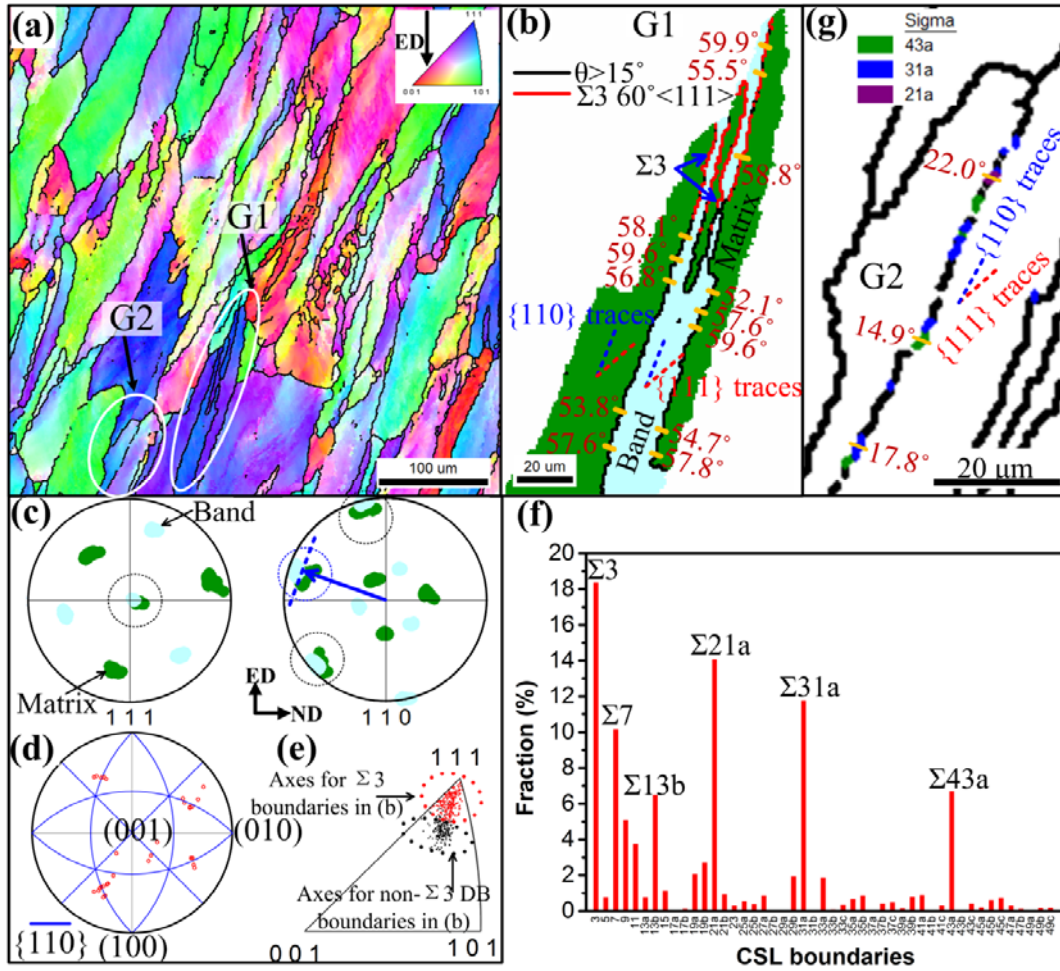## 3. Results and discussion

Fig. 3. (a) Orientation map of the 1P sample; (b) the selected grain G1; (c) pole figures of the DB and the matrix in (b); (d) the points of fifteen Σ3 boundary trace vectors on the (001) stereographic projection; (e) inverse pole figure showing the misorientation axes for the DB boundaries; (f) fraction of different CSL boundaries among total CSL boundaries; and (g) boundary map of the selected grain G2.

After one pass of ECAP (1P), typical microstructures in the longitudinal section are shown in Fig. 3(a). Most of the equiaxed grains are deformed into an elongated shape with an inclination angle of

~30˚ to the extrusion direction (ED). Interestingly, within some elongated coarse grains, twin-like lamellar grains delimited by high angle boundaries (HABs) can be observed and herein, we name them as deformation bands (DBs). As an example, the grain G1 highlighted by the white oval in Fig. 3(a) was magnified and shown in Fig. 3(b). Surprisingly, there are some Σ3 boundary segments (identified as 60˚<111> by the OIM software) coexisting with non-Σ3 general DB boundaries.

Fig. 3(c) shows the {111} and {110} poles of the DB and the matrix in Fig. 3(b). As can be identified, the DB and the matrix share one {111} pole and three sets of {110} poles, confirming that they have a Σ3 twin orientation relationship. However, as indicated in Fig. 3(b) and (c), the traces of DB boundaries are far way from {111} plane traces of both the DB and the matrix. Instead, they are closely parallel to one of the {110} plane traces. It indicates that these Σ3 DB boundary segments are not coherent deformation twin boundaries but ITBs. By using the single-section trace method [33], fifteeten Σ3 boundary segments (in different grains) were investigated and their poles were drawn in the (001) stereographic projection (Fig. 3(d)). Since the trace of each Σ3 boundary segment has two different indices belonging to the DB and the matrix, respectively, thus, 30 pole pionts were drawn. It can be seen that only 2 out of 30 points are positioned far away from the {110} traces, further revealing that most Σ3 boundaries are Σ3{110} ITBs. Furthermore, a distinct character of the DB boundaries is that their misorientation angles varies along their lengths. Based on statistical data, the misorientaions of non-Σ3 DB boundaries and Σ3 boundaries concentrate in the range of 50.0-60.3˚ and 54.1-60.4˚, respectively. Although some non-Σ3 DB boundaries are with misorientation angles matching the angle range of Σ3 boundaries (60.0 ± 8.7˚) [34], they cannot be identified as Σ3 boundaries because their misorientation axes are not <111> axes. This can be revealed by the inverse pole figure in Fig. 3(e), where the misorientation axes of the DB boundaries within G1 were collected. As can be seen, the misorientation axes of the non-Σ3 DB boundaries are far away from <111>.

Fractions of different CSL boundaries (based on three EBSD maps with the same magnification as Fig. 3(a)) have been calculated and shown in Fig. 3(f). As can be seen, some CSL boundaries are dominating, which have a common feature: <111> rotation axes. These boundaries include Σ3 60˚<111>, Σ7 38.2˚<111>, Σ13b 27.8˚<111>, Σ21a 21.8˚<111>, Σ31a 17.9˚<111> and Σ43a 15.2˚<111>. It implies that during deformation, CSL boundaries with low Σ values may have evolved

from CSL boundaries with higher Σ values by keeping the same rotation axes <111>. An example is shown in Fig. 3(g), within grain G2, Σ43a, Σ31a and Σ21a boundary segments coexist along one DB boundary, implying the possible transformation of Σ43a→Σ31a→Σ21a.
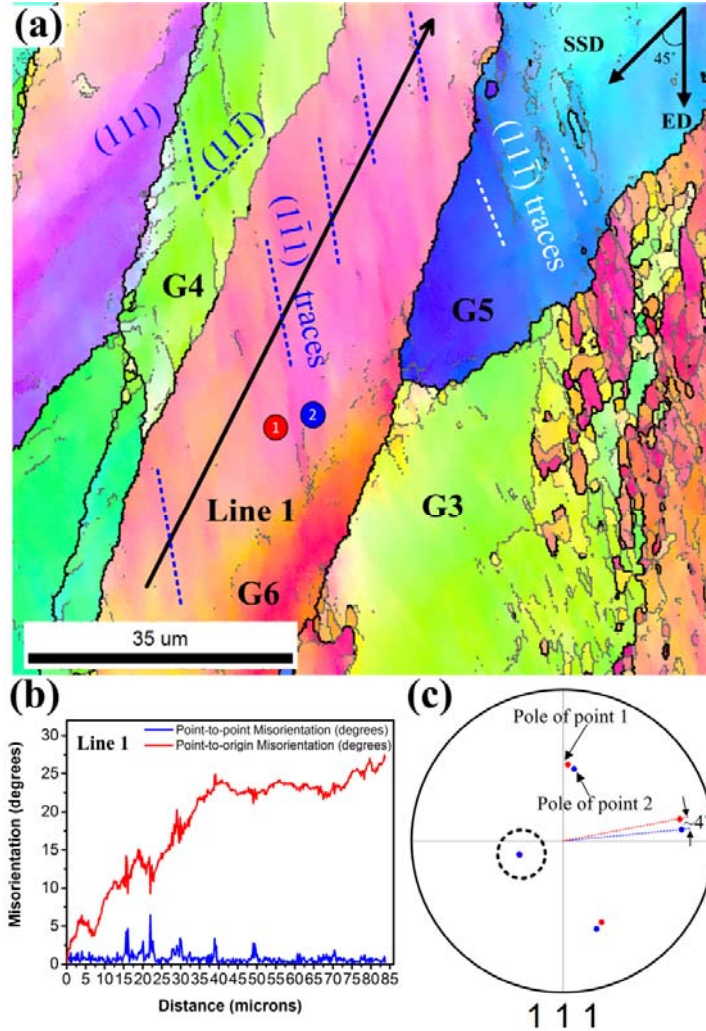

Fig. 4. (a) Orientation map of the 1P sample, where the grey and black lines depict boundaries with misorientation angles $5° \leq \theta < 15°$ and $\theta \geq 15°$, respectively; (b) misorientation profile along the Line 1 in (a); and (c) <111> pole figure of points 1 and 2 in (a). SSD is the abbreviation for simple shear direction.

Fig. 4(a) shows the deformation structure of elongated grains without Σ3 ITBs. As can be seen, inside some elongated grains, nearly equiaxed (sub)grains have formed, e.g., grain G3, while for the others, like grains G4-G6, only parallel DB boundaries with different misorientation angles can be observed. It is interesting to see that different from the well-developed ITBs shown in Fig. 3(b), the

DBs in G4-G6 (Fig. 4(a)) are delineated by LABs (< 15˚). The DB structure is similar to the cold rolled Al [35] and single crystal Al subjected to one pass of ECAP [30] that exhibit microstructures consisting of bands separated by geometrically necessary boundaries (GNBs) with {111} boundary planes. The formation and evolution of GNBs can accommodate the large strain gradients within grain interiors, which is mainly through self-organized glide on a single slip plane termed as planar slip [35, 36]. Within grain G6, non-uniformly spaced parallel DBs can be seen from the color difference although it is vaguely visible, which lie along the {111} traces. However, they are far away from the theoretical simple shear stress plane (45˚ to ED) of the 90˚ ECAP die, which indicates that GNB planes are not macroscopically aligned with the maximum stress direction.

The shear factors [30] of different {111} <$1\bar{1}0$> slip systems in G6 have been calculated. It shows that the slip system ($1\bar{1}1$) [110] has the highest shear factor value among all the slip systems, which is consistent with the experimental results shown in Fig. 4(a). It means that intensive dislocation slip occurs on the ($1\bar{1}1$) plane and the boundary planes of DBs tend to form on ($1\bar{1}1$), confirming that GNB planes are determined by the slip activity [37]. Misorientations along the elongated direction of grain G6 (along the Line 1) have been plotted in Fig. 4(b). Most point-to-point misorientations are less than 5.0˚. The point-to-origin misorientation curve shows the existence of a considerable long-range misorientation accumulation, implying that these DBs have formed by lattice rotation. As can be seen from Fig. 4(c), rotation axes of these DB boundaries are <111>, showing a characteristic of <111>-twist boundary.

The misorientations of GNBs are low-to-medium initially. The evolution of GNBs subjected to further deformation has been less studied. Fig. 5(a) shows another orientation map of the 1P sample. One of the grains G7 is enlarged and shown in Fig. 5(b), within which four well-developed DBs B1-B4 (the bands in green color) can be clearly seen. They appear as approximately parallel strips with widths of ~5-10 μm. From the local misorientations along the boundaries between B2 and the parent crystal, it can be seen that different segments have different misorientation angles, ranging from 8˚ to 51˚, implying that boundaries with higher misorientation angles have evolved from LABs. Furthermore, HAB segments are close to the {110} trace while the LAB segment encircled by the red

oval is closer to the {111} trace. This confirms that with increasing misorientation angles, the DB boundary planes evolve from {111} to {110} planes. As highlighted by the red rectangle in Fig. 5(b), Σ7 (38.2°<111>) boundary segments can also be found in the DB boundaries, indicating that CSL boundaries with <111> rotation axes have formed through the same deformation mechanism as the DB boundaries. However, as shown in Fig. 5(c), for the DB boundary segments with higher misorientations, the rotation axes are far away from <111> axes. In this case, the DB boundaries cannot evolve into Σ3 boundaries.
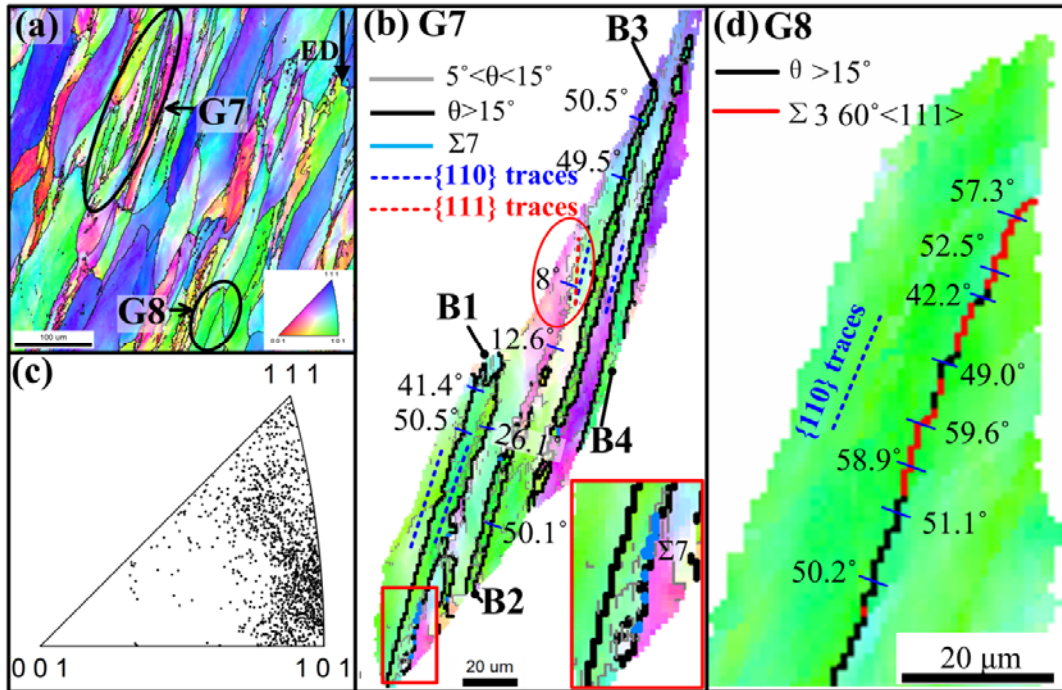

Fig. 5. (a) Orientation map of 1P sample showing selected grains comprising DBs; (b) the enlarged grain G7; (c) misorientation axes of DB boundaries in G7; and (d) the enlarged grain G8.

From the above analyses, considering that the Σ3{110} ITB segments are emerging in an alternative way with non-Σ3 DB boundaries with lower misorientaion anlges (for example, Fig. 5(d)), it can be confirmed that Σ3 ITBs have evolved from DB boundaries through dislocation slip. Note that for all the proposed twinning mechanisms of known twins, a fast nucleation process is always involved [7, 38] and the twin orientation relationship with respect to the grain matrix is achieved once the twin nucleates. Here, the formation of Σ3 ITBs in the present study is different. They have gradually evolved from DBs delineated by <111>-twist boundaries with {111} planes as boundary

planes. During deformation, through lattice rotation around the <111> axes, the DB boundaries evolve into CSL boundaries of Σ43a, Σ31a, Σ21a, Σ13b, Σ7 and finally Σ3 boundaries. However, with increasing misorientations, the boundary planes deviate from {111} planes and evolve into {110} planes. The alignment of boundary trace for DB boundaries with low misorietation angles (< 15˚) and high misorientation angles (> 15˚) to the extrution direction have been investigated in 15 and 20 grains, respevtively. As shown in Fig. 6, DB boundaries with high misorietation angles are close to the macroscopic elongation direction of grains (~30˚ to ED). It means that during continuous shearing of ECAP processing, DB boundary planes tend to rotate towards the elongation direction of grains. During this process, the boundary planes deviate from {111} planes to {110} planes, resulting in ITBs. However, during rotation, how the {111} boundary planes of LABs re-orientate exactly towards the {110} planes of the Σ3 ITBs (the smallest angle between {110} planes and the {111} planes is ~35.2˚) need more experimental and simulation work.
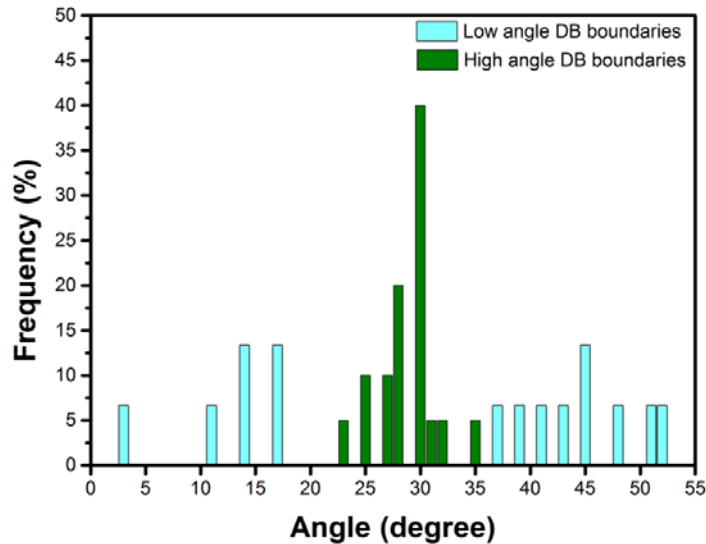

Fig. 6. The angle between DB boundary trace and the extrusion direction (ED) on the ND-ED plane.

In Ref [25], the formation of Σ3{112} ITBs in the Al-7Mg alloy has been attributed to the special planar glide deformation mode promoted by a high Mg content and the high strain rate (~10^2 s^{-1}) introduced by high impact loading. The tendency for planar glide increases with increasing solid solution contents or strain rates [39]. The high Mg content can promote the planar slip by decreasing

SFE and retarding dislocation motion. However, it has been suggested that SFE seems to be only of minor importance for the planar slip [39, 40]. Although Zn atoms are weaker than Mg atoms in terms of increasing the critical resolved shear stress of dislocation slip, they contribute to heterogeneous deformation and thus the formation of planar boundary until they reach high misorientation angles (the special case is 60˚<111>, i.e., Σ3 {110} ITBs). In the present study, even deformed at a quasi-static strain rate (ECAP), Σ3 ITBs can also be observed but with boundary planes on {110}, which is different from Σ3{112} ITBs reported in Ref. [25]. As has been suggested in Ref. [41], the formation of GNB planes can be related to co-directional slip distribution on two slip planes. By varying the slip proportions on the two slip planes of the co-directional slips, the boundary plane is changed accordingly. Therefore, any factors, including deformation methods, solute atoms and strain rates that alter the slip distribution on the two slip planes of a co-directional slip system can result in different GNB planes.

4. Conclusions

In summary, the present results demonstrate that parallel GNBs have formed in an Al-Zn alloy subjected to one pass of ECAP. At low misorientations, the boundary planes of GNBs are determined by slip activity, i.e., aligned with intensive {111} slip planes. With increasing misorientation angles, the GNBs evolve into <111>-twist CSL boundaries with different Σ values until Σ3 <111> boundaries. However, at higher misorientations, the boundary planes of GNBs deviate from {111} planes. The Σ3 boundaries have an incoherent twin nature, with {110} planes as boundary planes. This is a new deformation mechanism for Al alloys during ECAP, which has never been reported.

Acknowledgements

References

[1] X. Huang, N. Hansen, Grain orientation dependence of microstructure in aluminium deformed in tension, Scr. Mater. 37 (1997) 1-7.

[2] D.A. Hughes, N. Hansen, High angle boundaries formed by grain subdivision mechanisms, Acta Mater. 45 (1997) 3871-3886.

[3] B. Bay, N. Hansen, D.A. Hughes, D. Kuhlmann-Wilsdorf, Overview no. 96 evolution of f.c.c. deformation structures in polyslip, Acta Metall. Mater. 40 (1992) 205-219.

[4] J.A. Wert, Q. Liu, N. Hansen, Dislocation boundaries and active slip systems, Acta Metall. Mater. 43 (1995) 4153-4163.

[5] X.L. Wu, X.Z. Liao, S.G. Srinivasan, F. Zhou, E.J. Lavernia, R.Z. Valiev, Y.T. Zhu, New Deformation Twinning Mechanism Generates Zero Macroscopic Strain in Nanocrystalline Metals, Phys. Rev. Lett. 100 (2008) 095701.

[6] M.A. Meyers, O. Vöhringer, V.A. Lubarda, The onset of twinning in metals: a constitutive description, Acta Mater. 49 (2001) 4025-4039.

[7] J.W. Christian, S. Mahajan, Deformation twinning, Prog. Mater. Sci. 39 (1995) 1-157.

[8] K. Lu, L. Lu, S. Suresh, Strengthening Materials by Engineering Coherent Internal Boundaries at the Nanoscale, Science 324 (2009) 349-352.

[9] L. Lu, Y.F. Shen, X.H. Chen, L.H. Qian, K. Lu, Ultrahigh strength and high electrical conductivity in copper, Science 304 (2004) 422-426.

[10] M. Dao, L. Lu, Y.F. Shen, S. Suresh, Strength, strain-rate sensitivity and ductility of copper with nanoscale twins, Acta Mater. 54 (2006) 5421-5432.

[11] R.J. Asaro, Y. Kulkarni, Are rate sensitivity and strength effected by cross-slip in nano-twinned fcc metals, Scr. Mater. 58 (2008) 389-392.

[12] Y. Zhang, Y. Li, N.R. Tao, K. Lu, High strength and high electrical conductivity in bulk nanograined Cu embedded with nanoscale twins, Appl. Phys. Lett. 91 (2007) 211901-211901-211903.

[13] A.J. Cao, Y.G. Wei, S.X. Mao, Deformation mechanisms of face-centered-cubic metal nanowires with twin boundaries, Appl. Phys. Lett. 90 (2007) 151909.

[14] L. Lu, R. Schwaiger, Z.W. Shan, M. Dao, K. Lu, S. Suresh, Nano-sized twins induce high rate sensitivity of flow stress in pure copper, Acta Mater. 53 (2005) 2169-2179.

[15] S. Hai, E.B. Tadmor, Deformation twinning at aluminum crack tips, Acta Mater. 51 (2003) 117-131.

[16] B.Q. Li, M.L. Sui, B. Li, E. Ma, S.X. Mao, Reversible Twinning in Pure Aluminum, Phys. Rev. Lett. 102 (2009) 205504.

[17] Y.S. Li, N.R. Tao, K. Lu, Microstructural evolution and nanostructure formation in copper during dynamic plastic deformation at cryogenic temperatures, Acta Mater. 56 (2008) 230-241.

[18] M. Chen, E. Ma, K.J. Hemker, H. Sheng, Y. Wang, X. Cheng, Deformation twinning in nanocrystalline aluminum, Science 300 (2003) 1275-1277.

[19] Y.T. Zhu, X.Z. Liao, X.L. Wu, Deformation twinning in nanocrystalline materials, Prog. Mater. Sci. 57 (2012) 1-62.

[20] X.Z. Liao, F. Zhou, E.J. Lavernia, D.W. He, Y.T. Zhu, Deformation twins in nanocrystalline Al, Appl. Phys. Lett. 83 (2003) 5062-5064.

[21] X.Z. Liao, Y.H. Zhao, S.G. Srinivasan, Y.T. Zhu, R.Z. Valiev, D.V. Gunderov, Deformation twinning in nanocrystalline copper at room temperature and low strain rate, Appl. Phys. Lett. 84 (2004) 592-594.

[22] X.Z. Liao, F. Zhou, E.J. Lavernia, S.G. Srinivasan, M.I. Baskes, D.W. He, Y.T. Zhu, Deformation mechanism in nanocrystalline Al: Partial dislocation slip, Appl. Phys. Lett. 83 (2003) 632-634.

[23] M. Muzyk, Z. Pakiela, K.J. Kurzydlowski, Ab initio calculations of the generalized stacking fault energy in aluminium alloys, Scr. Mater. 64 (2011) 916-918.

[24] D.D. Zhao, O.M. Løvvik, K. Marthinsen, Y.J. Li, Impurity effect of Mg on the generalized planar fault energy of Al, J. Mater. Sci. 51 (2016) 6552-6568.

[25] S.B. Jin, K. Zhang, R. Bjørge, N.R. Tao, K. Marthinsen, K. Lu, Y.J. Li, Formation of incoherent deformation twin boundaries in a coarse-grained Al-7Mg alloy, Appl. Phys. Lett. 107 (2015) 091901.

[26] H.L. Jia, R. Bjørge, K. Marthinsen, Y.J. Li, The deformation and work hardening behaviour of a SPD processed Al-5Cu alloy, J. Alloys Compd. 697 (2017) 239-248.

[27] H.L. Jia, R. Bjørge, K. Marthinsen, R.H. Mathiesen, Y.J. Li, Soft particles assisted grain refinement and strengthening of an Al-Bi-Zn alloy subjected to ECAP, Mater. Sci. Eng. A 703 (2017) 304-313.

[28] H.L. Jia, K. Marthinsen, Y.J. Li, Effect of soft Bi particles on grain refinement during severe plastic deformation, Trans. Nonferrous Met. Soc. China 27 (2017) 971-976.

[29] M. Zha, Y.J. Li, R.H. Mathiesen, R. Bjørge, H.J. Roven, Microstructure evolution and mechanical behavior of a binary Al–7Mg alloy processed by equal-channel angular pressing, Acta Mater. 84 (2015) 42-54.

[30] Y. Fukuda, K. Oh-ishi, M. Furukawa, Z. Horita, T.G. Langdon, The application of equal-channel angular pressing to an aluminum single crystal, Acta Mater. 52 (2004) 1387-1395.

[31] Y. Fukuda, K. Oh-ishi, M. Furukawa, Z. Horita, T.G. Langdon, Influence of crystal orientation on ECAP of aluminum single crystals, Mater. Sci. Eng. A 420 (2006) 79-86.

[32] R.Z. Valiev, T.G. Langdon, Principles of equal-channel angular pressing as a processing tool for grain refinement, Prog. Mater. Sci. 51 (2006) 881-981.

[33] P.H. Pumphrey, K.M. Bowkett, Axis/angle pair description of coincidence site lattice grain boundaries, Scr. Metall. 5 (1971) 365-369.

[34] D.G. Brandon, The structure of high-angle grain boundaries, Acta Metall. 14 (1966) 1479-1484.

[35] C. Hong, X. Huang, G. Winther, Dislocation content of geometrically necessary boundaries aligned with slip planes in rolled aluminium, Philos. Mag. 93 (2013) 3118-3141.

[36] D.A. Hughes, N. Hansen, D.J. Bammann, Geometrically necessary boundaries, incidental dislocation boundaries and geometrically necessary dislocations, Scr. Mater. 48 (2003) 147-153.

[37] G. Winther, D.J. Jensen, N. Hansen, Dense dislocation walls and microbands aligned with slip planes-theoretical considerations, Acta Mater. 45 (1997) 5059-5068.

[38] J.Z. Zhao, L. Ratke, Modelling of rapid unidirectional solidification of hypermonotectic alloys, Mater. Lett. 38 (1999) 235-238.

[39] D.A. Hughes, Microstructural evolution in a non-cell forming metal: Al-Mg, Acta Metall. Mater. 41 (1993) 1421-1430.

[40] V. Gerold, H.P. Karnthaler, On the origin of planar slip in f.c.c. alloys, Acta Metall. 37 (1989) 2177-2183.

[41] G. Winther, X. Huang, Dislocation structures. Part II. Slip system dependence, Philos. Mag. 87 (2007) 5215-5235.

Figure captions:

Fig. 1. Microstructures of the as-cast Al-8Zn alloy. (a) EBSD map and (b) grain size distribution chart.

Fig. 2. (a) Schematic diagram of the ECAP die, (b) sketch of the sample for ECAP and the region for EBSD observation is also indicated. ND, TD and ED are abbreviations of the normal, transverse and extrusion directions, respectively.

Fig. 3. (a) Orientation map of the 1P sample; (b) the selected grain G1; (c) pole figures of the DB and the matrix in (b); (d) the points of fifteen Σ3 boundary trace vectors on the (001) stereographic projection; (e) inverse pole figure showing the misorientation axes for the DB boundaries; (f) fraction of different CSL boundaries among total CSL boundaries; and (g) boundary map of the selected grain G2.

Fig. 4. (a) Orientation map of the 1P sample, where the grey and black lines depict boundaries with misorientation angles $5° \leq \theta < 15°$ and $\theta \geq 15°$, respectively; (b) misorientation profile along the Line 1 in (a); and (c) <111> pole figure of points 1 and 2 in (a). SSD is the abbreviation for simple shear direction.

Fig. 5. (a) Orientation map of 1P sample showing selected grains comprising DBs; (b) the enlarged grain G7; (c) misorientation axes of DB boundaries in G7; and (d) the enlarged grain G8.

Fig. 6. The angle between DB boundary trace and the extrusion direction (ED) on the ND-ED plane.